J|A|C|S COMMUNICATIONS

Published on Web 01/13/2009

Structured Mesoporous Tin Oxide with Electrical Conductivity. Application in Electroluminescence

Carmela Aprile, Laura Teruel, Mercedes Alvaro, and Hermenegildo Garcia*

Instituto de Tecnología Quimica CSIC-UPV, Av. de los Naranjos s/n, Universidad Politécnica de Valencia, 46022 Valencia, Spain

Received September 10, 2008; E-mail: hgarcia@qim.upv.es

One of the problems limiting application in microtechnology of periodic mesoporous silica (PMS) thin films is their lack of electrical conductivity. Insulating PMS hosts constitute a barrier impeding the charge transport between external working electrodes and the guests incorporated within the PMS mesopores. Applications in electronic circuits, electrochemical sensors, electroluminescent films, and photovoltaic cells will largely benefit of the use of conductive mesoporous hosts.[1]

Herein we describe the synthesis of an electrically conductive periodic mesoporous oxide based on the structuring of tin oxide nanoparticles. In addition to providing direct conductivity measurements, we illustrate with an example the advantage of a conductive material with respect to conventional insulator PMS.

Tin oxide is one of the most common metal oxides behaving as electrical conductor.[2] On the basis of this property, we prepared small tin oxide nanoparticles that can serve as building blocks for the preparation of mesoporous solids. Tin oxide nanoparticles of 2−5 nm were prepared by hydrolysis of $SnCl_4$. The particle size distribution was determined by TEM (see Supporting Information).

Recently small nanoparticles instead of molecular compounds have been used as building blocks for the synthesis of mesoporous materials.[3,4] These nanoparticles can be used in combination of molecular precursors that favor nanoparticle connectivity, material robustness, and structural stability.[4] Besides, the presence of molecular precursors assist templation by efficient interaction with the structure directing agent.

According to these lines, we have used tin oxide nanoparticles in the presence of tetraethyl orthosilicate (TEOS, 50 wt %) or in its absence to prepare structured mesoporous materials. Using cetyltrimethylammonium bromide (CTAB) as structure directing agent and effecting the synthesis under basic conditions, two solids $mpSnO_2$-100 and $mpSnO_2$-50 (mp stands for mesoporous and the number indicates SnO_2 weight percentage) were prepared. For the sake of comparison, in the present work we have also used an all-silica mesoporous MCM-41 material and the properties of these mesoporous solids were compared to that of the unstructured nanoparticles ($preSnO_2$, "pre" denoting that these nanoparticles were the precursors of $mpSnO_2$). Table 1 lists the main textural and porosity data for these four materials.

XRD shows for MCM-41 its expected periodic hexagonal structuring. Also for $mpSnO_2$-50, the (100) diffraction peak was observed at 2.0° (insert in Figure 1). However, $mpSnO_2$-100 did not exhibit low angle diffraction peaks indicating that if TEOS is absent in the synthesis gel, CTAB does not template pre-SnO_2 nanoparticles into a periodic material.

Isothermal N_2 sorption measurements shows for $mpSnO_2$-50 mononodal pore diameter and about nine times larger surface area than $preSnO_2$ (see Figure 1 and Table 1). Interestingly, as it can be seen in Figure 1, $mpSnO_2$-100 also exhibits the typical isothermal gas adsorption characteristic of mesoporous solids with bimodal pore size distribution. The gas sorption hysteresis loop observed for $mpSnO_2$-100 indicates a cage-like mesoporous structure, showing that lyotropic liquid crystals of the CTAB surfactant has been able to create mesoporosity in $mpSnO_2$-100.

Table 1. Composition and Porosity Data of the Materials Used in This Work

	template	SnO_2/TEOS content (wt %)	pore size (Å)	BET surface area ($m^2 \times g^{-1}$)
$preSnO_2$		100/0		40
$mpSnO_2$-50	CTAB	50/50	33	357
$mpSnO_2$-100	CTAB	100/0	37/78	94
MCM-41	CTAB	0/100	32	986

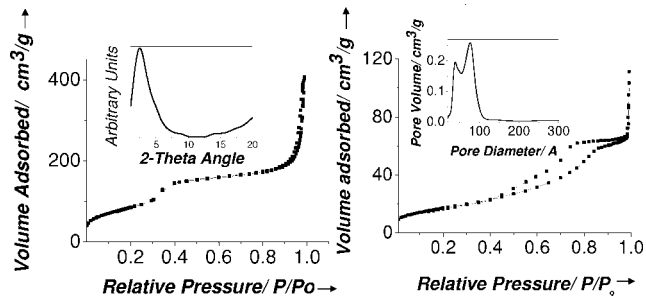

Figure 1. N_2 sorption isotherms of $mpSnO_2$-50 (left) and $mpSnO_2$-100 (right). The left inset shows an expansion of $mpSnO_2$-50 low-angle XRD and the inset on the right the bimodal pore distribution of $mpSnO_2$-100.

The BET surface area of $mpSnO_2$-100 is significantly lower than $mpSnO_2$-50 (see Table 1), reflecting the lack of periodic ordering when no TEOS is added to the synthesis gel.

Porosity of $mpSnO_2$-100 and $mpSnO_2$-50 can be observed by TEM (Figure 2). Thus, front and side TEM views of $mpSnO_2$-50 channels show that the solid is constituted by an array of fairly regular, parallel channels. More interestingly, TEM images of $mpSnO_2$-100 clearly reveal the presence of uniform mesopores. The characterization data presented show that both $mpSnO_2$-50 and $mpSnO_2$-100 are mesoporous materials having similar narrow pore size distribution, the main difference being the periodic long-range ordering present in $mpSnO_2$-50 and absent in $mpSnO_2$-100. The latter material has mesoporous cages as previously observed for related mesoporous materials that do not exhibit XRD.[5] Periodicity and high BET area can be positive for those properties not affected by the presence of silica domains.

Conductivity measurements were undertaken in the total absence of moisture. $mpSnO_2$-100 exhibits the highest conductivity that is over 9 orders of magnitude higher than that of all-silica MCM-41 (Figure 3). The presence of silica in the structure is highly detrimental for the electrical conductivity as shown by the 3 orders of magnitude higher resistivity of $mpSnO_2$-50 compared to $mpSnO_2$-

10.1021/ja807190j CCC: $40.75

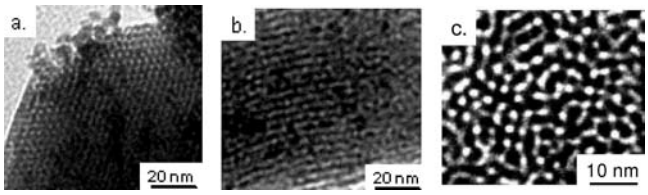

Figure 2. TEM images showing front (a) and parallel (b) views of mpSnO_2-50 and the homogeneous pore size structure of mpSnO_2-100 (c).

100. Importantly, the resistivity of mpSnO_2-100 in the 0.7−2.2 V range is over 3-fold lower than that of preSnO_2. The higher conductivity of mpSnO_2-100 over preSnO_2 arises most probably from the spatial nanoparticle ordering, the presence of porosity, and the larger surface area. In our knowledge, the data of Figure 3 correspond by far to the lowest resistive mesoporous host reported up to now.

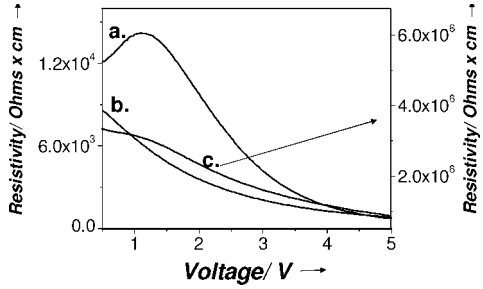

Figure 3. Resistivity−voltage plot for preSnO_2 nanoparticles (a), mpSnO_2-100 (b), and mpSnO_2-50 (c) recorded at room temperature under vacuum in a sealed cell after dehydration at 400 °C for 1 h. Note the different vertical scales.

One potential application of conductive mesoporous materials is electroluminescence. As we said, guest encapsulation in insulating PMS hosts results in poor charge transport from external electrodes to the guest located in the host pores. Thus, encapsulation inside insulator PMS negatively affects guest electroluminescence. To show the advantage of conductive mesoporous materials for host−guest electroluminescent materials, we prepared poly(1,4-dimethoxy-*p*-phenylenevinylene) conducting polymer (dMeOPPV) inside mpSnO_2 mesopores. Peparation consisted in the preadsorption the 2,5-bis(chloromethyl)-1,4-dimethoxybenzene monomer followed by basic polymerization inside the channels using K^{t}BuO (eq 1).[6]

$$\text{monomer@mpSnO}_2 \xrightarrow[\text{THF}]{^t\text{ButOK}} \text{dMeOPPV@mpSnO}_2 \qquad (1)$$

Polymer formation was confirmed by optical spectroscopy in where the characteristic absorption band of the red dMeOPPV polymer appears around 480 nm (see Figure 4 inset). Combustion chemical analysis established that the dMeOPPV loading in mpSnO_2-100 was 12 wt %. For comparison, we prepared materials at identical loadings in where dMeOPPV was hosted in MCM-41, mpSnO_2-50 and adsorbed on preSnO_2 nanoparticles.

With the dMeOPPV-containing materials, electroluminescent cells were prepared with the following configuration: FTO/(dMeOPPV)@host/Al (see Supporting Information). The remarkable benefit of the electrical conductivity was reflected by the fact that below 10 V (dMeOPPV)@mpSnO_2-100 was the only material exhibiting electroluminescence (Figure 4). The emission turn-on voltage for dMeOPPV@mpSnO_2-100 was 4 V and the emission intensity grows in the 4−10 V DC range. In the case of mpSnO_2-50 when the cell voltage was above 10 V electroluminescence was also observed with much lower relative efficiency. For dMeOPPV-preSnO_2 current flow through the cell was observed at voltages above 10 V, but no light emission could be ever detected. Importantly, using MCM-41 as host no light emission or current flow was observed under any circumstance.

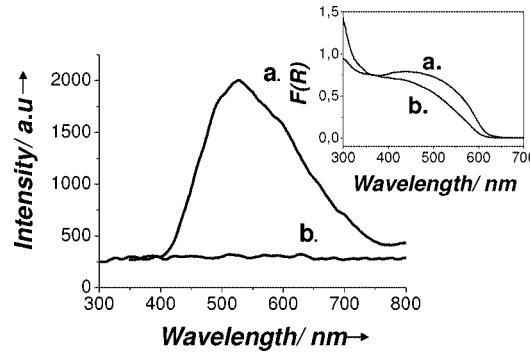

Figure 4. Electroluminescence spectra of dMeOPPV incorporated in mpSnO_2-100 (a) and mpSnO_2-50 (b) at 7 V. The inset shows the diffuse reflectance optical spectra of dMeOPPV in mpSnO_2 (a) and preSnO_2 (b).

In summary, structured mesoporous tin oxides exhibit over 9 orders of magnitude higher electrical conductivity than mesoporous silicas. Spatial structuring and surface area increases the electrical conductivity of the material that is higher than that of the precursor SnO_2 nanoparticles. The advantage of having electrically conductive mesoporous hosts for applications requiring charge transport from external electrodes has been proven by observation of low turn-on voltage electroluminescence from a conjugated PPV polymer incorporated in the porous solids. Also for this application, the unstructured precursor SnO_2 nanoparticles or insulating PMSs are inactive.

Acknowledgment. Dedicated to Prof. J. Font on the occasion of his 65th birthday. Financial support by the Spanish DCI (CTQ06-06785) is gratefully acknowledged. C.A. thanks the Spanish Ministry of Education for a Juan de la Cierva research associate contract.

Supporting Information Available: Experimental section, SnO_2 nanoparticle synthesis, mpSnO_2 synthesis, electrical conductivity measurements, electroluminescent cells preparation. This material is available free of charge via the Internet at http://pubs.acs.org.

References

(1) Moller, K.; Bein, T. *Chem. Mater.* **1998**, *10*, 2950–2963. Bein, T. *Stud. Surf. Sci. Catal.* **2007**, *168*, 611–657. Behrens, P. *Adv. Mater.* **1993**, *5*, 127–132. Nicole, L.; Boissiere, C.; Grosso, D.; Quach, A.; Sanchez, C. *J. Mater. Chem.* **2005**, *15*, 3598–3627. Hoffmann, F.; Cornelius, M.; Morell, J.; Froba, M. *Angew. Chem., Int. Ed.* **2006**, *45*, 3216–3251. Inagaki, S.; Guan, S. *Mater. Res. Soc. Symp. Proc.* **2002**, *726*, 225–233. Scott, B. J.; Wirnsberger, G.; Stucky, G. D. *Chem. Mater.* **2001**, *13*, 3140–3150.
(2) Exarhos, G. J.; Zhou, X. D. *Thin Solid Films* **2007**, *515*, 7025–7052.
(3) Fan, H. Y. *Chem. Commun.* **2008**, *138*, 3–1394. Mukherjee, S.; Kim, K.; Nair, S. *J. Am. Chem. Soc.* **2007**, *129*, 6820–6826. Warren, S. C.; Disalvo, F. J.; Wiesner, U. *Nat. Mater.* **2007**, *6*, 156–U123. de Soler-Illia, G. J.; Sanchez, C.; Lebeau, B.; Patarin, J. *Chem. Rev.* **2002**, *102*, 4093–4138. Wright, A.; Gabaldon, J.; Burckel, D. B.; Jiang, Y. B.; Tian, Z. R.; Liu, J.; Brinker, C. J.; Fan, H. Y. *Chem. Mater.* **2006**, *18*, 3034–3038.
(4) Alvaro, M.; Aprile, C.; Garcia, H.; Gomez-Garcia, C. J. *Adv. Funct. Mater.* **2006**, *16*, 1543–1548.
(5) Li, F.; Wang, Z. Y.; Ergang, N. S.; Fyfe, C. A.; Stein, A. *Langmuir* **2007**, *23*, 3996–4004. Thommes, M.; Smarsly, B.; Groenewolt, M.; Ravikovitch, P. I.; Neimark, A. V. *Langmuir* **2006**, *22*, 756–764.
(6) Kraft, A.; Grimsdale, A. C.; Holmes, A. B. *Angew. Chem., Int. Ed.* **1998**, *37*, 403–428.

JA807190J